Geophysical Research Letters

RESEARCH LETTER
10.1029/2023GL103855

Siege in the Southern Stratosphere: Hunga Tonga-Hunga Ha'apai Water Vapor Excluded From the 2022 Antarctic Polar Vortex

Gloria L. Manney[1,2], Michelle L. Santee[3], Alyn Lambert[3], Luis F. Millán[3], Ken Minschwaner[2], Frank Werner[3], Zachary D. Lawrence[4,5], William G. Read[3], Nathaniel J. Livesey[3], and Tao Wang[3]

[1]NorthWest Research Associates, Socorro, NM, USA, [2]New Mexico Institute of Mining and Technology, Socorro, NM, USA, [3]Jet Propulsion Laboratory, California Institute of Technology, Pasadena, CA, USA, [4]Cooperative Institute for Research in Environmental Sciences (CIRES) & NOAA Physical Sciences Laboratory (PSL), University of Colorado, Boulder, CO, USA, [5]NorthWest Research Associates, Boulder, CO, USA

Abstract We use Aura Microwave Limb Sounder (MLS) trace gas measurements to investigate whether water vapor (H_2O) injected into the stratosphere by the Hunga Tonga-Hunga Ha'apai (HTHH) eruption affected the 2022 Antarctic stratospheric vortex. Other MLS-measured long-lived species are used to distinguish high HTHH H_2O from that descending in the vortex from the upper-stratospheric H_2O peak. HTHH H_2O reached high southern latitudes in June–July but was effectively excluded from the vortex by the strong transport barrier at its edge. MLS H_2O, nitric acid, chlorine species, and ozone within the 2022 Antarctic polar vortex were near average; the vortex was large, strong, and long-lived, but not exceptionally so. There is thus no clear evidence of HTHH influence on the 2022 Antarctic vortex or its composition. Substantial impacts on the stratospheric polar vortices are expected in succeeding years since the H_2O injected by HTHH has spread globally.

Plain Language Summary The 2022 Hunga Tonga-Hunga Ha'apai eruption injected vast amounts of water vapor into the stratosphere. Concern arose that this excess water vapor could affect the 2022 Antarctic stratospheric polar vortex and ozone hole: Water vapor plays a crucial role in forming polar stratospheric clouds, which provide surfaces upon which chemical reactions that destroy ozone take place. Enhanced water vapor also affects temperatures, which in turn affect the powerful winds defining the polar vortex boundary. Antarctic polar vortex development began in April–May; by June the intense vortex-edge winds presented a formidable obstacle to transport. Satellite trace-gas measurements show that when water vapor from the Hunga Tonga eruption reached the vortex edge in June, it faced an impenetrable barrier and "besieged" the vortex, building up exceptionally strong water vapor gradients across the vortex edge. Water vapor, ozone, and chemicals involved in ozone destruction remained near historical average levels within the vortex through spring 2022. Because excess water vapor spread throughout the south polar regions after vortex breakup, much larger effects on the Antarctic vortex and chemical processing within it are expected in 2023 and beyond, when high water vapor will be entrained into the vortex as it develops.

Key Points:

- Microwave Limb Sounder (MLS) trace gas data show that the Hunga Tonga-Hunga Ha'apai H_2O plume was effectively excluded from the 2022 Antarctic polar vortex
- Antarctic lower stratospheric vortex strength, size, and longevity were among the largest on record, but within the range of previous years
- Antarctic chemical ozone loss in 2022 was unexceptional, with MLS ozone and related trace gases observed to be near average

Supporting Information:

Supporting Information may be found in the online version of this article.

Correspondence to:

G. L. Manney,
manney@nwra.com

Citation:

Manney, G. L., Santee, M. L., Lambert, A., Millán, L. F., Minschwaner, K., Werner, F., et al. (2023). Siege in the southern stratosphere: Hunga Tonga-Hunga Ha'apai water vapor excluded from the 2022 Antarctic polar vortex. *Geophysical Research Letters*, *50*, e2023GL103855. https://doi.org/10.1029/2023GL103855

Received 24 MAR 2023
Accepted 4 JUL 2023

Author Contributions:

Conceptualization: Gloria L. Manney, Michelle L. Santee
Formal analysis: Gloria L. Manney, Alyn Lambert
Investigation: Gloria L. Manney, Michelle L. Santee, Alyn Lambert, Luis F. Millán, Ken Minschwaner, Frank Werner, Zachary D. Lawrence, William G. Read, Nathaniel J. Livesey, Tao Wang
Methodology: Gloria L. Manney, Alyn Lambert, Zachary D. Lawrence

1. Introduction

The 15 January 2022 eruption of the underwater volcano Hunga Tonga-Hunga Ha'apai (HTHH) injected an unprecedented amount of water vapor (H_2O) directly into the stratosphere, increasing the stratospheric H_2O burden by approximately 10% (e.g., Millán et al., 2022; Vömel et al., 2022). It also resulted in substantial, though not unprecedented, enhancements in volcanic aerosol loading (Khaykin et al., 2022; Sellitto et al., 2022; Taha et al., 2022). Numerous studies have already explored aspects of the stratospheric impacts of HTHH enhancements in aerosol and H_2O; of particular relevance here are suggestions that H_2O and aerosol from HTHH injected into the Southern Hemisphere (SH) stratosphere took many months to reach high latitudes and did not extend poleward of about 60°S (e.g., Khaykin et al., 2022; Legras et al., 2022; Schoeberl et al., 2022; Zhu et al., 2022). In the lowermost stratosphere (at and below approximately the 380 K isentropic surface), a few studies suggest that some H_2O and aerosol may have been transported to high SH latitudes within days to weeks via the shallow branch of the Brewer-Dobson circulation (e.g., Khaykin et al., 2022; Schoeberl et al., 2022; Taha et al., 2022). Radiative cooling from HTHH H_2O led to unprecedented cold in SH middle and low latitudes, with associated circulation and transport anomalies in that region (Coy et al., 2022; Schoeberl et al., 2022; Sellitto et al., 2022).

Software: Gloria L. Manney, Luis F. Millán, Zachary D. Lawrence, Nathaniel J. Livesey
Validation: Luis F. Millán, Frank Werner, William G. Read, Nathaniel J. Livesey, Tao Wang
Visualization: Gloria L. Manney
Writing – original draft: Gloria L. Manney
Writing – review & editing: Gloria L. Manney, Michelle L. Santee, Alyn Lambert, Luis F. Millán, Ken Minschwaner, Frank Werner, Zachary D. Lawrence, William G. Read, Nathaniel J. Livesey, Tao Wang

It was suggested that HTHH aerosol and H_2O transported into high SH latitudes might impact the composition of the 2022 SH stratospheric polar vortex and that circulation changes associated with HTHH H_2O might affect the strength, size, and/or longevity of that vortex (e.g., Taha et al., 2022; Zhu et al., 2022). However, the Antarctic stratospheric polar vortex presents a strong transport barrier (e.g., Schoeberl et al., 1992; Schoeberl & Hartmann, 1991), so any possible impacts would depend on the timing of vortex formation and arrival of the HTHH plume at the vortex edge, and on potential impacts of the H_2O plume on vortex strength via radiative processes that result in circulation changes. Here we use Aura Microwave Limb Sounder (MLS) data to analyze the evolution of the SH polar vortex in 2022, transport of HTHH H_2O in relation to it, and chemical processing within it. We use H_2O, nitrous oxide (N_2O), nitric acid (HNO_3), carbon monoxide (CO), hydrogen chloride (HCl), chlorine monoxide (ClO), and ozone (O_3) from version 5 (v5) MLS "level 2" (L2) and "level 3" (L3) data (Livesey et al., 2020), along with meteorological fields from NASA's Modern Era Retrospective-analysis for Research and Applications Version 2 (MERRA-2) data set (Gelaro et al., 2017; Global Modeling and Assimilation Office (GMAO), 2015).

Immediately following the eruption, standard MLS v5 quality screening (Livesey et al., 2020) flagged many of the profiles most affected by HTHH as suspect retrievals (Millán et al., 2022); thus H_2O and N_2O anomalies shown here may be artificially small for up to 3 weeks after the eruption. Since our focus is on subsequent transport and the relationship to the SH polar vortex, our results are unaffected. MERRA-2 radiative heating rates may also be inaccurate since MERRA-2 does not assimilate stratospheric H_2O and thus does not represent well the impact of HTHH H_2O on radiative heating (e.g., Coy et al., 2022); however, the circulation anomalies shown by Coy et al. (2022) were confined to latitudes well equatorward of the vortex edge, suggesting that this is not expected to substantially impact our results for the southern polar regions.

2. Transport of HTHH Stratospheric H_2O

Figure 1 shows several views of the evolution of N_2O and H_2O (both generally long-lived transport tracers in the stratosphere) anomalies in the SH lower and middle stratosphere: vortex averages as a function of potential temperature (θ); on isentropic (constant θ) surfaces as a function of equivalent latitude (EqL, the latitude enclosing the same area between it and the pole as a given potential vorticity, PV, contour, Butchart & Remsberg, 1986); and on selected dates as a function of EqL and θ. The years shown in the time series include ones with exceptionally warm/short-lived (2019) and cold/long-lived (2020 and 2021) springtime polar vortices, as well as a more typical year (2018) (WMO, 2023). The Supporting Information S1 shows the full MLS H_2O fields at Figure 1 levels and on the days in the EqL/θ snapshots (Figure S1 in Supporting Information S1), and EqL time series at levels in the lower stratosphere of anomaly fields for each species over the full Aura mission (Figures S2–S4 in Supporting Information S1). Also shown in Figures S2–S4 in Supporting Information S1 are EqL time series of anomalies in two mixing diagnostics, effective diffusivity (Nakamura, 1996) and scaled PV (sPV) gradients. Figure S5 in Supporting Information S1 shows EqL/θ anomaly plots in 2020 for comparison with Figure 1.

The evolution of vortex-averaged N_2O (Figure 1a) in 2022 was unexceptional, with positive anomalies above ~430 K matched or exceeded by those in several previous years in the MLS record (see, e.g., Figure S2 in Supporting Information S1 at 550 K). The vertical dipole pattern of vortex N_2O anomalies is common, and higher values in 2020, 2021, and 2022 were consistent with lower vortex temperatures and accompanying weaker diabatic descent (e.g., Figure S6 in Supporting Information S1). N_2O EqL/time evolution (Figures 1b–1d) is also largely typical: Outside the vortex at 550 and 700 K, recurring changes from high to low anomalies extending from low latitudes show quasi-biennial oscillation (QBO) related transport (e.g., Baldwin et al., 2001; Diallo et al., 2019). While high extravortex N_2O anomalies from ~550 to 700 K during the 2022 winter (Figures 1b and 1c, 1m–1p) are matched or exceeded in several previous years (Figure S2 in Supporting Information S1), they are also consistent with the anomalous midlatitude circulation (diagnosed by, e.g., Coy et al., 2022) arising from persistent HTHH-related midlatitude cold anomalies (e.g., Coy et al., 2022; Schoeberl et al., 2022). Low N_2O anomalies along the vortex edge in austral spring 2020 and 2021 indicate low N_2O remaining confined later into spring in more persistent vortices in those years (see also Figure S5 in Supporting Information S1 for 2020). Similar, but weaker, vortex-edge N_2O anomalies in spring 2022 suggest a long-lived vortex. In contrast, high vortex-edge N_2O anomalies in spring 2019 resulted from a rare SH sudden stratospheric warming that led to a small, warm, short-lived vortex (e.g., Wargan et al., 2020). Mixing diagnostics (Figures S2–S3 in Supporting Information S1) show low effective diffusivity and high sPV gradient anomalies along the vortex edge after June in 2020, 2021, and 2022, indicating a later than usual vortex breakdown, consistent with the N_2O evolution.

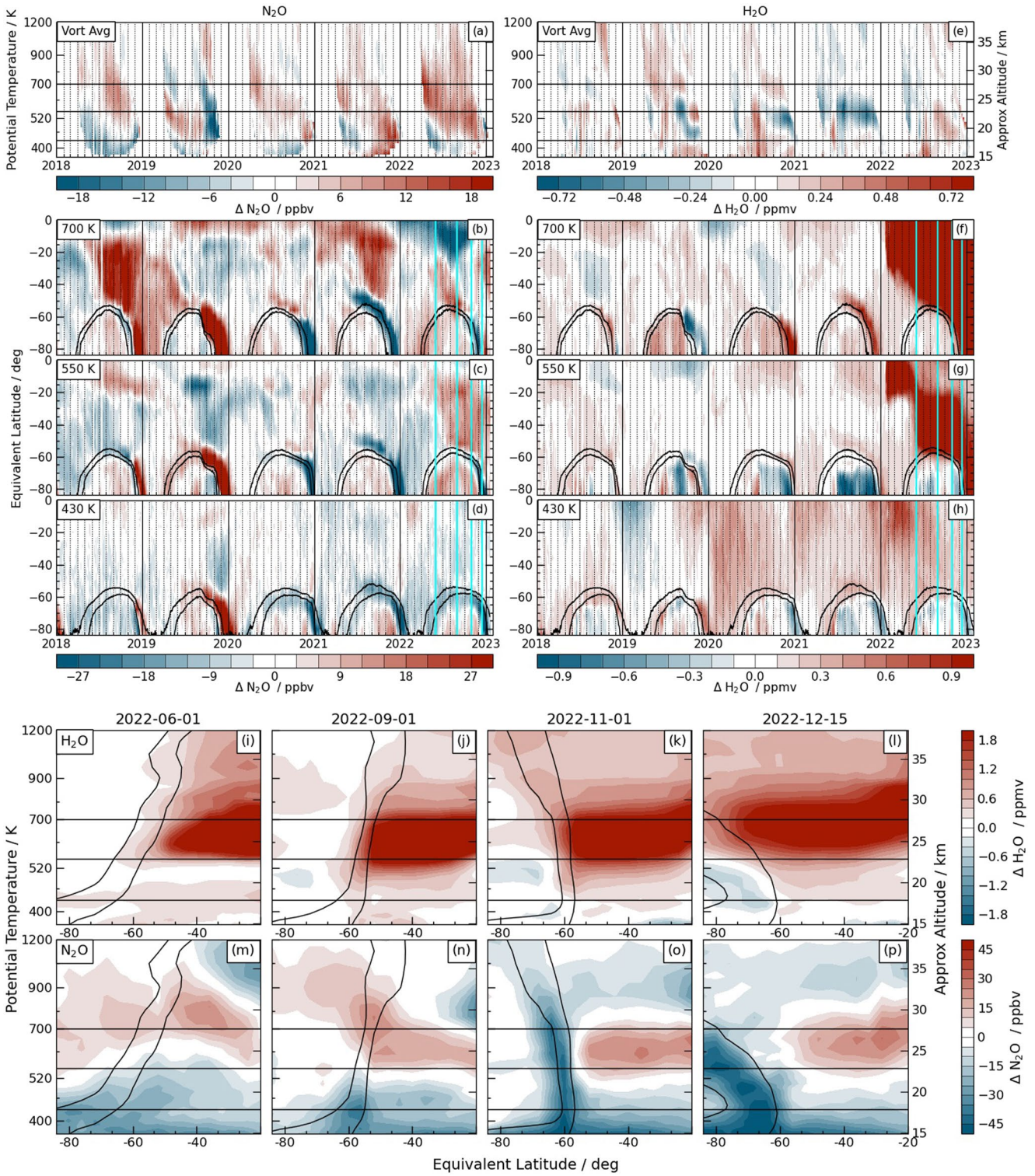

Figure 1. Evolution of MLS-observed SH anomalies from the baseline 2005–2021 climatology of N_2O (a–d, m–p) and H_2O (e–h, i–l) from January 2018 through January 2023: (a, e) vortex-averaged values; (b–d, f–h) evolution as a function of EqL at levels in the middle through lower stratosphere (horizontal lines in a, e, i–p): 700 K (~26–28 km), 550 K (~21–23 km), and 430 K (~16–18 km); (i–p) EqL/θ snapshots on four representative days (vertical cyan lines in EqL/time plots). Black contours in b–d, f–h, and i–p are scaled PV (sPV; scaled to have a similar range of values throughout the stratosphere, e.g., Dunkerton & Delisi, 1986; Manney et al., 1994) values indicating the vortex edge region. The vortex edge is defined as in Lawrence et al. (2018) using sPV values in the region of strongest PV gradients. Approximate altitudes (a, e, i–p) are calculated per Knox (1998).

H_2O anomalies (Figures 1e–1h) in the SH lower stratospheric vortex typically reflect interannual variations in polar stratospheric cloud (PSC) extent; low H_2O anomalies in spring 2020 and 2021 (Figure 1e) over ∼450–650 K arose from more persistent PSC activity in unusually long-lasting vortices. Outside the vortex (Figures 1f–1h), high H_2O anomalies often accompany low N_2O anomalies because H_2O and N_2O have opposite vertical and horizontal gradients in the lower to middle stratosphere. For example, low (high) springtime H_2O (N_2O) anomalies appeared along the vortex edge in 2019, with opposite patterns in 2020 and 2021 at 550–700 K; similar patterns occurred in mid-EqLs in earlier years (Figure S2 in Supporting Information S1) and are consistent with the mixing anomalies (Figures S2–S4 in Supporting Information S1), which suggest stronger and longer-lasting vortices in those years. Above ∼500 K, typical signatures of extravortex transport of H_2O are overwhelmed by the arrival of HTHH H_2O (Figures 1f and 1g; Figure S2 in Supporting Information S1). HTHH H_2O reached the vortex edge in early June 2022, after the vortex was fully developed except in the lowermost stratosphere (below ∼400 K). Subsequently, extremely strong H_2O gradients developed along the vortex edge over 520–800 K and persisted through October or later, into December below ∼700 K (Figures 1f and 1g, 1i–1l). These exceptionally strong gradients suggest that the HTHH plume could not penetrate the vortex. Pervasive high H_2O anomalies since early 2020 below ∼500 K (e.g., Figure 1h) may reflect lingering enhancements from the 2020 Australian New Years fires (e.g., Santee et al., 2022). While small positive anomalies appear to encroach into the vortex region in late winter 2022 at and below 500 K, similar features are common (e.g., in 2018 and 2021), so it is unclear whether they are related to the HTHH plume. At all levels examined (including the lowermost stratosphere, e.g., Figure S4 in Supporting Information S1), H_2O anomalies inside the vortex are within the typical range. By mid-December, only a weak remnant of the vortex remained below ∼520 K; above that level the H_2O enhancement filled the south polar region (Figures 1f, 1g, and 1l). MLS data thus show no indication of air from the HTHH H_2O plume penetrating into the SH vortex before its breakup.

EqL time series and cross-sections of OMPS-LP aerosol (Figures S7–S8 in Supporting Information S1) appear consistent with the results for H_2O, except for a suggestion of early arrival of aerosol at high southern latitudes in the lowermost stratosphere (below ∼400 K) in March–May, before vortex formation at these levels (consistent with Taha et al., 2022; Schoeberl et al., 2022; Khaykin et al., 2022); it is unclear whether any of this enhanced aerosol in the lowermost stratosphere is entrained into the lowest reaches of the vortex, which does not fully develop until July at those levels (e.g., Santee et al., 2011).

The above results provide visual evidence that the vortex edge presented an effective transport barrier, preventing substantial penetration of the vortex by the HTHH H_2O plume from June into November. To look more closely at the robustness of the vortex edge as a transport barrier, Figure 2 shows scatter plots of H_2O versus N_2O and sPV for representative days in 2022 compared with the evolution in all prior years in the MLS record. Low N_2O (relative to the range of values at a given level) and high-magnitude sPV identify vortex air parcels. In the lower stratosphere (exemplified by 550 K), increasingly low vortex H_2O through the season results from dehydration and is very similar to that previously observed by MLS (density plots, Figure S9 in Supporting Information S1, emphasize the similarity of the main distributions in 2022 to those in earlier years). Extravortex H_2O at 550 K does not stand out from the previous record before July; thereafter, the HTHH enhancement manifests as a distinct cluster of high H_2O with N_2O near 200 ppbv and sPV magnitudes $<1 \times 10^{-4}$ s^{-1} (both values that are unambiguously extravortex) that is unique to 2022 (compare yellow-orange/purple H_2O/sPV values with gray dots in Figure 2; orange with gray contours in Figure S9 in Supporting Information S1).

In the middle stratosphere (exemplified by 700 K), vortex H_2O values first increase via descent of the upper stratospheric peak, then decrease as continuing descent brings low mesospheric H_2O into the stratospheric vortex (e.g., Lee et al., 2011; Ray et al., 2002); both the high (e.g., Figures 2a and 2b) and the low (e.g., Figures 2c and 2f) H_2O values that descend through the vortex (low N_2O, high-magnitude sPV end of the *x*-axis) at 700 K are distinct from the extravortex population of high H_2O from HTHH, and that is in turn distinguished from extravortex air in previous years by higher H_2O values at extravortex N_2O (∼150–200 ppbv) and lower-magnitude sPV (magnitude $<\sim 1 \times 10^{-4}$ s^{-1}). Density plots versus sPV (Figures S9d–S9f, S9j–S9l in Supporting Information S1) particularly highlight this separation. These correlations of H_2O with N_2O and sPV demonstrate that the air with enhanced H_2O from HTHH remained well separated from that within the vortex until vortex breakup at each level (as suggested in Figure S1 in Supporting Information S1 and Figure 1). MLS H_2O/CO correlations show a similar picture in the middle and upper stratosphere (e.g., Figure S10 in Supporting Information S1), with HTHH H_2O associated with low CO values characteristic of extravortex air.

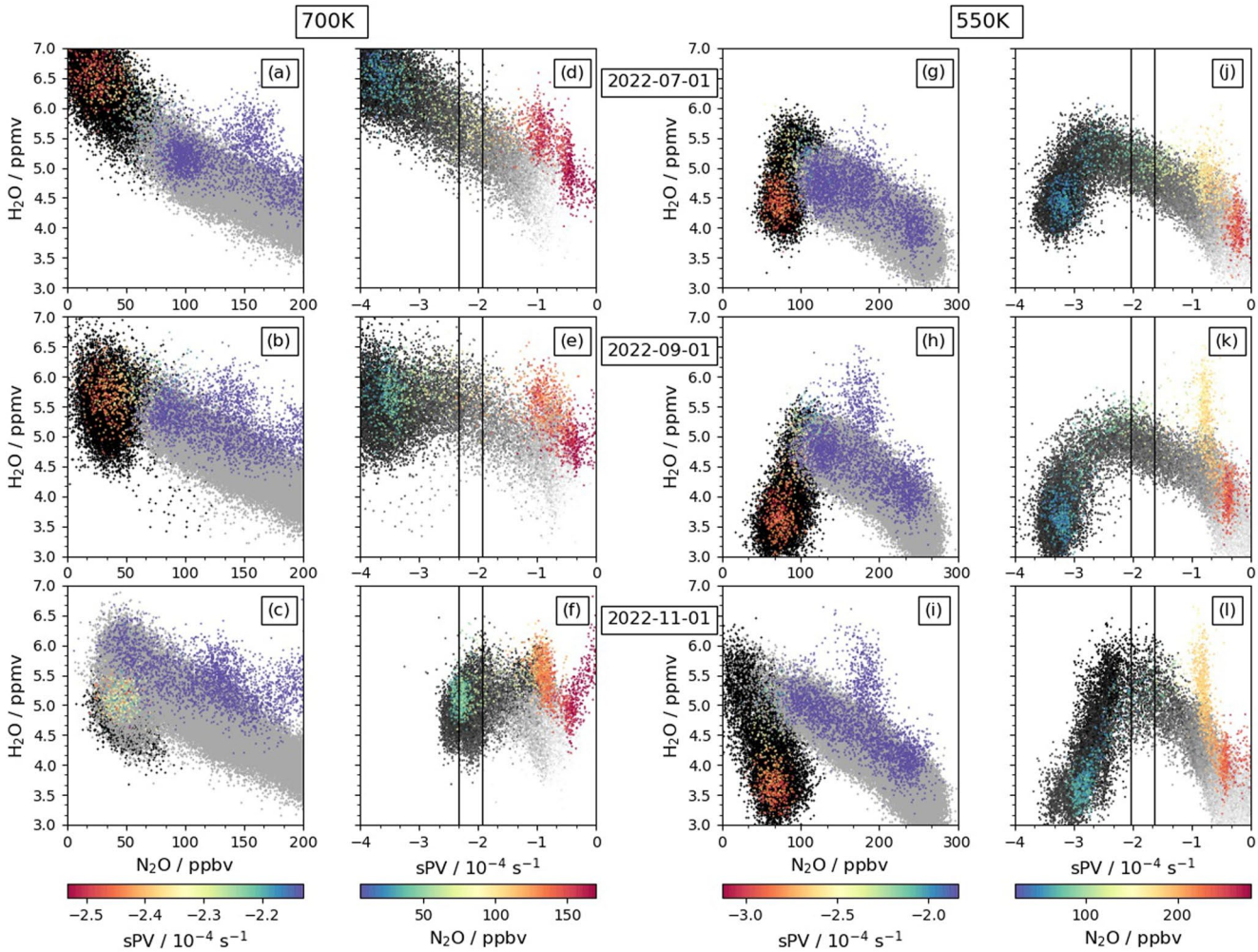

Figure 2. Scatter plots of MLS H_2O (*y*-axis) versus N_2O (a–c, g–i) and sPV (d–f, j–l). Gray and black dots show values from 2005 to 2021; for those years, black (gray) indicates *x*-axis values of N_2O or sPV characteristic of inside (outside) the vortex. For 2022, colored (purple) dots show sPV values inside (outside) the vortex. 2022 N_2O is colored such that blue/blue-green (yellow/orange/red) shows typical vortex (extravortex) values. Black vertical lines on the plots versus sPV indicate the vortex edge region. Left two columns show 700 K (~26–28 km) and right two columns 550 K (~21–23 km).

Because the seawater from HTHH has a higher ratio of HDO to H_2O than background water vapor in the extravortex stratosphere (e.g., Khaykin et al., 2022; Randel et al., 2012), examining this ratio (termed ΔD herein, calculated from Atmospheric Chemistry Experiment-Fourier Transform spectrometer HDO and H_2O as in Randel et al., 2012) provides further indication of the separation of the HTHH plume from vortex air (Figures S11–S12 in Supporting Information S1). An unprecedented increase in this ratio was seen in SH midlatitudes; in the lower stratosphere, ΔD was higher in the HTHH plume than in the vortex, and relatively high vortex ΔD values are associated with low, rather than high, H_2O. While vortex ΔD values in the middle stratosphere are climatologically high (e.g., Randel et al., 2012) and are associated with relatively high H_2O, that distribution was clearly separated from the high ΔD/high H_2O HTHH plume, which was excluded from the vortex (Figure S12 in Supporting Information S1).

3. Composition and Vortex Chemical Processing

Figure 3 shows MLS O_3, as well as the reservoir chlorine species HCl and the active (O_3-destroying) chlorine species ClO. (Figures S2–S3 in Supporting Information S1 show EqL/time plots of these species at 550 and 430 K, and Figure S4 in Supporting Information S1 shows O_3 at 380 K, for the full mission. Figure S5 in Supporting Information S1 shows EqL/θ snapshots like those in Figure 3 but for 2020). The Antarctic vortex was

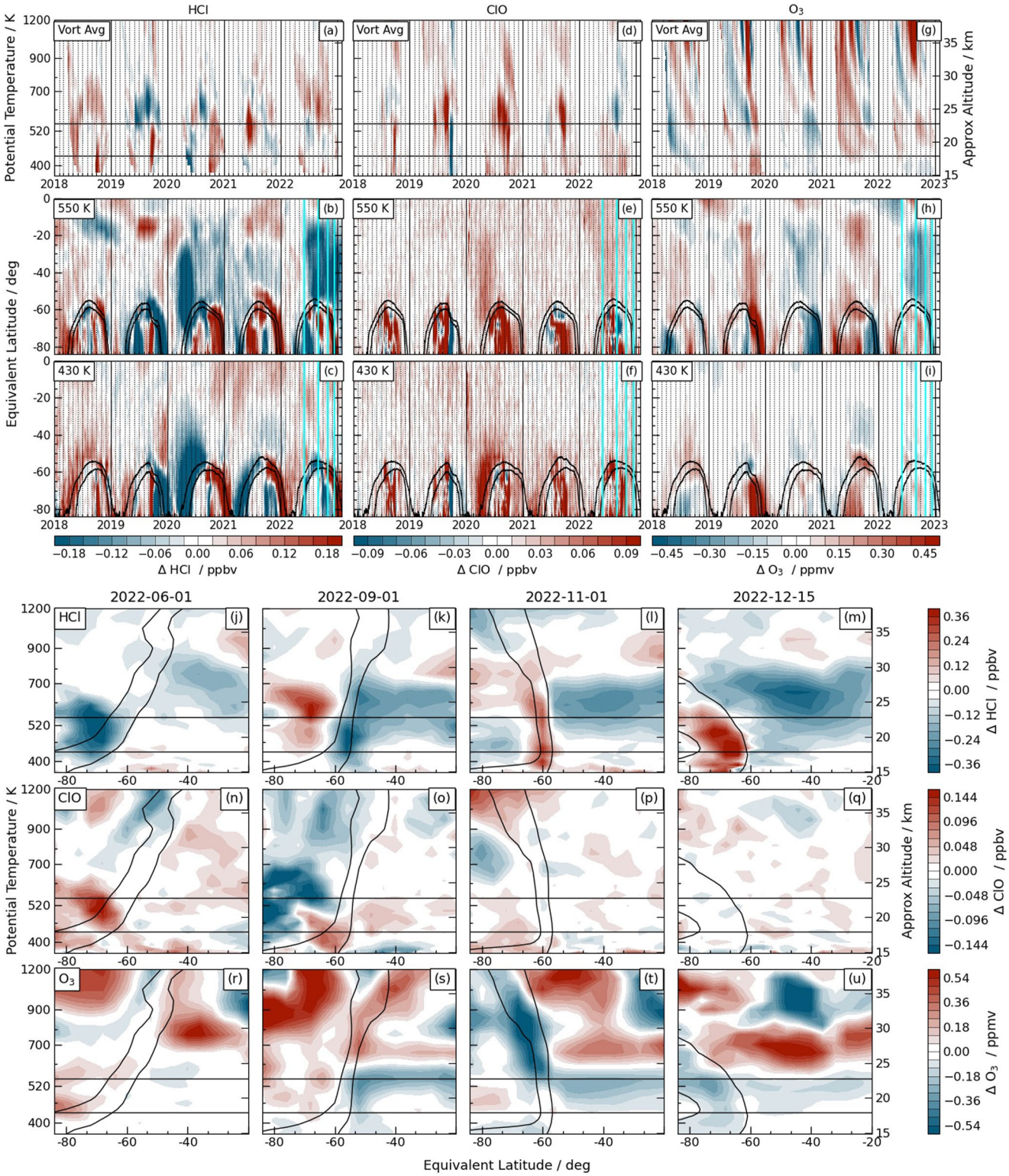

Figure 3. As in Figure 1, but for MLS (a–c, j–m) HCl, (d–f, n–q) ClO, and (g–i, r–u) O_3; (a, d, g) vortex averages, (b, e, h) 550 K (~21–23 km) and (c, f, i) 430 K (~16–18 km) EqL time series; and (j–u) EqL/θ snapshots.

unusually persistent in spring 2022, but less so than in 2020 and 2021. Vortex HCl and ClO commonly oscillate between high and low anomalies during a given cold season; the 2022 vortex was no exception, with low (high) HCl (ClO) anomalies during much (but not all, e.g., Figures 3k and 3o) of the season. High HCl anomalies appeared along the vortex edge in November and in the vortex remnant in mid-December, consistent with high values resulting from deactivation into HCl (as is typical in the SH, e.g., Santee et al., 2008). The persistence of these values resulted from unusually enduring confinement in a vortex that broke down later in spring than is typical; similar, but stronger, HCl anomalies were seen in the 2020 and 2021 vortices (Figures 3b and 3c; also see Figure S5 in Supporting Information S1 for 2020), reflecting as late or later vortex persistence in those years.

Consistent with near-average vortex values of the chlorine species, O_3 anomalies in 2022 were also small. Lower-stratospheric O_3 anomalies in early winter (before extensive chemical loss) were slightly positive and remained so through October (see, e.g., Figures 3r and 3s). Both 2020 and 2021 showed lower O_3 and earlier onset of low ozone anomalies, consistent with colder and longer-lived (see below) vortices in those years than in 2022. Small low O_3 anomalies in mid-December 2022 are consistent with the extended persistence of the vortex (a weaker echo of those in 2020, Figure S5 in Supporting Information S1, when vortex temperatures were lower and the vortex persisted even longer). Outside the vortex, low HCl and O_3 anomalies are consistent with the high N_2O anomalies (e.g., Figures 1c, 1m–1p) and with midlatitude temperature and circulation anomalies arising from radiative effects of HTHH H_2O (e.g., Coy et al., 2022; Schoeberl et al., 2022), suggesting that transport plays a key role in these perturbations. It is unclear whether some HTHH aerosol may have been entrained into the lowest reaches of the vortex (below ~400 K) as it formed (Figures S7–S8 in Supporting Information S1); however, the MLS data show no evidence of unusual polar processing even at those lowest levels. The results in Figure 3 thus indicate that the modest low anomalies in O_3 seen in austral spring 2022 result primarily (if not entirely) from the unusual persistence of the vortex.

4. Vortex Evolution and Trace Gas Confinement

Figure 4 summarizes the evolution of the 2022 SH lower stratospheric vortex relative to the 43-year MERRA-2 record and the evolution of trace gases relative to the 18-year MLS record. Figure S13 in Supporting Information S1 shows profiles of additional MERRA-2 diagnostics of vortex strength and longevity. Consistent with indications in trace gases of its unusual persistence, the 2022 SH spring vortex was among the largest on record up to ~650 K, approximately matching the maximum size and persistence seen prior to 2020 (Figures 4a–4c; Figures S13b–S13d in Supporting Information S1). In spring, the 2021 vortex area was slightly larger and the 2020 vortex area substantially larger than that in 2022 over ~460–650 K, with record lower-stratospheric vortex persistence in 2020 (Figures 4a–4c, Figures S13b–S13d in Supporting Information S1). Maximum PV gradients, indicating vortex strength (i.e., robustness as a transport barrier), show unusually strong springtime vortices in 2020 through 2022 below ~500 K, but only the 2020 vortex was stronger than average above ~600 K (Figures 4d–4f; Figure S13a in Supporting Information S1). Below ~520 K, the area with temperatures below the nitric acid trihydrate (NAT) PSC threshold was larger than usual (Figure 4g) and PSCs persisted later than usual (Figures 4g and 4h, Figures S13e–S13h in Supporting Information S1) in 2020, 2021, and 2022, but only exceeded previous springtime records in 2020; above ~600 K PSC area and duration were near average (Figure 4, Figures S13e–S13h in Supporting Information S1). MLS vortex-averaged temperatures (Figures S14i–S14l in Supporting Information S1) were near one standard deviation below the mean in October/November (similar to those in 2020 and 2021), but near average earlier in the winter.

The unexceptional MLS trace gas evolution in the 2022 Antarctic vortex is highlighted in Figures 4j–4u (Figure S14 in Supporting Information S1 shows the vertical structure, as well as additional fields including temperature and HNO_3). Interannual variability in SH polar chemical processing is relatively small, but, with few exceptions, all of the trace gases show 2022 evolution that is well within the previously observed range. Over ~450–600 K, persistently low H_2O after October in 2022, and to an even greater extent in 2020 and 2021, is consistent with confinement of dehydrated air in long-lived vortices. Chlorine evolution (seen in HCl and ClO, Figures 4m–4r; Figures S14q–S14x in Supporting Information S1) was fairly typical throughout the season, as was that of HNO_3 (Figures S14m–S14p in Supporting Information S1). Observed O_3 evolution in 2022 was remarkably near average throughout the season (Figures 4s–4u; Figures S14y–S14B in Supporting Information S1).

5. Summary

The unprecedented water vapor injection into the stratosphere by HTHH is tracked using MLS and reanalysis data. The H_2O from HTHH arrived at the vortex edge in early June and, to use a military metaphor, laid siege to

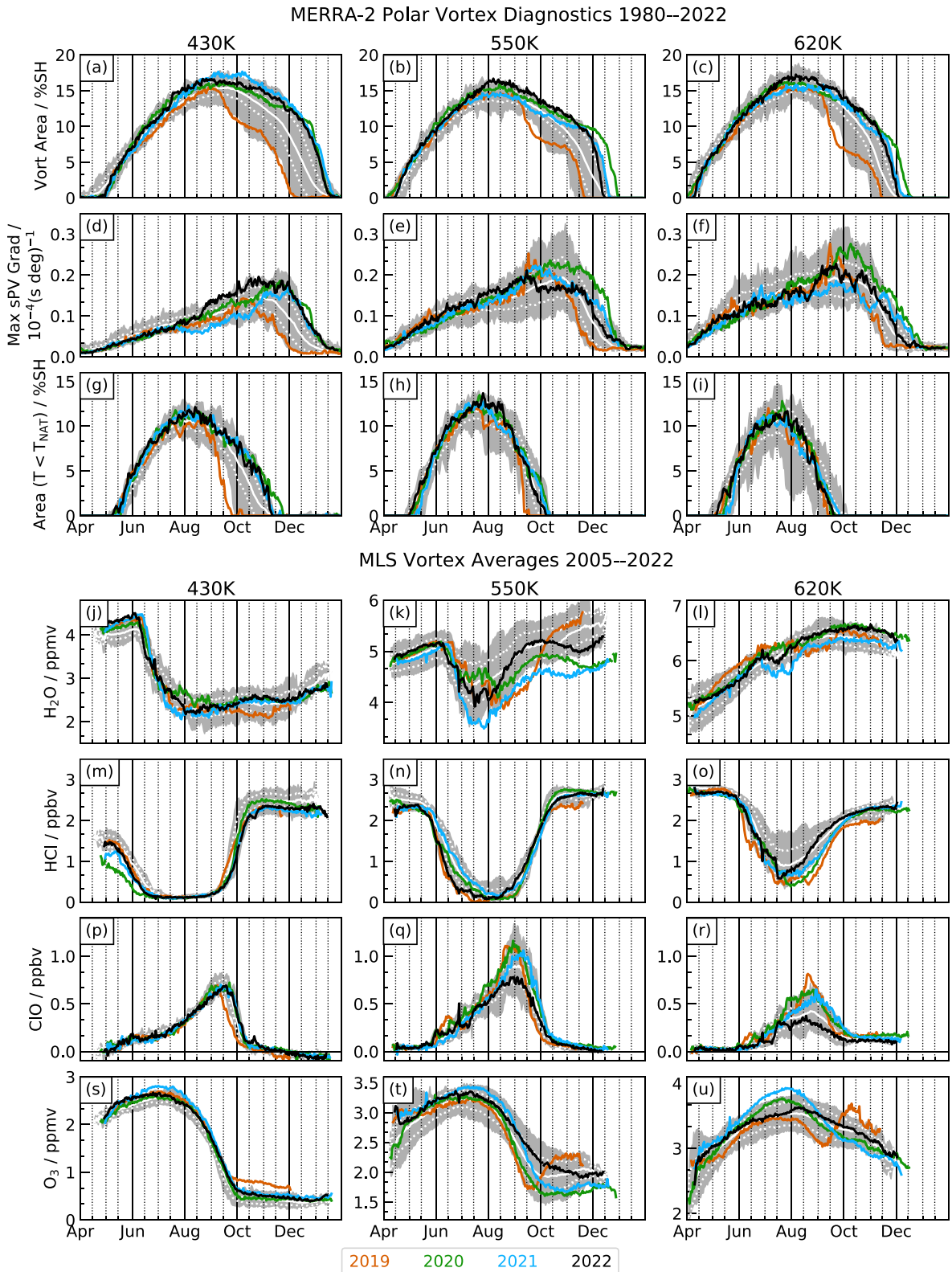

Figure 4. Time series at three levels in the lower stratosphere of (a–c) vortex area, (d–f) maximum PV gradients, and (g–i) area below the NAT PSC threshold, comparing 2019 (orange), 2020 (green), 2021 (cyan), and 2022 (black) with the range (shading), mean (solid white line), and one standard deviation envelope (dotted white lines) over 1980–2018. Vortex-averaged MLS (j–l) H_2O, (m–o) HCl, (p–r) ClO, and (s–u) O_3 in same format, with the range being over 2005–2018. Levels shown are 430 K (~16–18 km), 550 K (~21–23 km), and 620 K (~24–25 km).

it, building up exceptionally strong gradients across the vortex edge that persisted into November. The transport barrier remained largely impermeable, preventing the plume from penetrating into the vortex until it broke down in November to December. In contrast to speculation that HTHH stratospheric H_2O and aerosol injections would lead to substantial anomalies in the Antarctic polar vortex and lower stratospheric polar processing and ozone loss within it (e.g., Taha et al., 2022; Zhu et al., 2022), our analysis suggests that HTHH did not cause notable changes: Aura MLS HCl, ClO, and O_3 concentrations inside the vortex through the depth of the lower stratosphere all show evolution well within the range of previous years during the Aura mission, with near-average O_3 loss. There is likewise no unequivocal evidence for dynamical impacts on the vortex: The vortex was among the larger, stronger, and longer-lived in the SH lower stratosphere, but these conditions were matched or exceeded by those in 2020, 2021, and several previous years in the MERRA-2 record since 1980; vortex cold anomalies were even less exceptional. Therefore, despite large radiative, dynamical, and composition perturbations in midlatitudes, the observational evidence shows that chemical processing within the 2022 Antarctic stratospheric polar vortex was fairly typical, with no clear indications of dynamical vortex perturbations. Any possible impacts on the 2022 Antarctic vortex were thus sufficiently subtle that comprehensive modeling efforts would be needed to attribute them to HTHH.

The spread of the HTHH H_2O into polar latitudes following the Antarctic vortex breakup (e.g., Figure 1) led to unprecedented high H_2O anomalies throughout the SH, which are expected to linger for at least several years (e.g., Khaykin et al., 2022; Millán et al., 2022), raising the expectation of large perturbations to Antarctic polar vortex chemistry and the ozone hole in 2023 and beyond. HTHH H_2O has also been transported into the Northern Hemisphere (e.g., Schoeberl et al., 2023), but reached the Arctic vortex edge after the vortex was well-developed and was only dispersed through the Northern Hemisphere after a strong sudden stratospheric warming starting in mid-February (paper in preparation). Thus large effects on Arctic polar vortex chemistry are also expected to manifest starting in the 2023/2024 cool season.

Data Availability Statement

The data used herein are publicly available as follows:

- MERRA-2 (Global Modeling and Assimilation Office (GMAO), 2015): https://disc.gsfc.nasa.gov/datasets/M2I3NVASM_5.12.4/summary?keywords=M2I3NVASM_5.12.4
- Aura MLS Level-2 and Level-3 data (Lambert et al., 2021a, 2021b; Lambert, Livesey, & Read, 2020; Lambert, Read, & Livesey, 2020; Manney et al., 2021; Santee et al., 2021; Schwartz et al., 2020; Schwartz, Froidevaux, et al., 2021; Schwartz, Livesey, et al., 2021) https://disc.gsfc.nasa.gov/datasets?page=1&source=Aura%20MLS
- ACE-FTS v4.1/4.2 data: http://www.ace.uwaterloo.ca (registration required)
- ACE-FTS v4.1/4.2 error flags (Sheese & Walker, 2020): https://doi.org/10.5683/SP2/BC4ATC
- MLS and ACE-FTS derived meteorological products (DMPs; Manney & Millán, 2007–present): https://mls.jpl.nasa.gov/eos-aura-mls/dmp (registration required)
- OMPS-LP NASA (Taha, 2020): https://doi.org/10.5067/CX2B9NW6FI27
- OMPS-LP USask (Zawada et al., 2022): https://doi.org/10.5281/zenodo.7293121.

Acknowledgments
Thanks to the MLS team at JPL for data processing and analysis support, especially Brian Knosp for data management, Ryan Fuller for development and production of the MLS L3 products, Lucien Froidevaux and Michael Schwartz for helpful discussions. Thanks to two anonymous reviewers for their helpful comments. Thanks to the ACE science team for making the ACE-FTS data available, especially Kaley Walker and Patrick Sheese for advice on data quality and usage. Thanks to the GMAO for providing the MERRA-2 data set. G.L. Manney was supported by the Jet Propulsion Laboratory (JPL) Microwave Limb Sounder team under JPL subcontract #1521127 to NWRA. Work at the Jet Propulsion Laboratory, California Institute of Technology, was carried out under a contract with the National Aeronautics and Space Administration (80NM0018D0004).

References

Baldwin, M. P., Gray, L. J., Dunkerton, T. J., Hamilton, K., Haynes, P. H., J, W., et al. (2001). The quasi-biennial oscillation. *Reviews of Geophysics*, *39*(2), 179–229. https://doi.org/10.1029/1999rg000073

Butchart, N., & Remsberg, E. E. (1986). The area of the stratospheric polar vortex as a diagnostic for tracer transport on an isentropic surface. *Journal of the Atmospheric Sciences*, *43*(13), 1319–1339. https://doi.org/10.1175/1520-0469(1986)043<1319:taotsp>2.0.co;2

Coy, L., Newman, P. A., Wargan, K., Partyka, G., Strahan, S. E., & Pawson, S. (2022). Stratospheric circulation changes associated with the Hunga Tonga-Hunga Ha'apai eruption. *Geophysical Research Letters*, *49*(22), e2022GL100982. https://doi.org/10.1029/2022GL100982

Diallo, M., Konopka, P., Santee, M. L., Müller, R., Tao, M., Walker, K. A., et al. (2019). Structural changes in the shallow and transition branch of the Brewer–Dobson circulation induced by El Niño. *Atmospheric Chemistry and Physics*, *19*(1), 425–446. https://doi.org/10.5194/acp-19-425-2019

Dunkerton, T. J., & Delisi, D. P. (1986). Evolution of potential vorticity in the winter stratosphere of January-February 1979. *Journal of Geophysical Research*, *91*(D1), 1199–1208. https://doi.org/10.1029/jd091id01p01199

Gelaro, R., McCarty, W., Suárez, M. J., Todling, R., Molod, A., Takacs, L., et al. (2017). The modern-era retrospective analysis for research and applications, version-2 (MERRA-2). *Journal of Climate*, *30*(14), 5419–5454. https://doi.org/10.1175/JCLI-D-16-0758.1

Global Modeling and Assimilation Office (GMAO). (2015). MERRA-2 inst3_3d_asm_nv: 3d, 3-hourly,instantaneous, model-level, assimilation, assimilated meteorological fields v5.12.4 [Dataset]. Goddard Earth Sciences Data and Information Services Center (GES DISC). https://doi.org/10.5067/WWQSXQ8IVFW8

Khaykin, S., Podglajen, A., Ploeger, F., Grooß, J.-U., Tence, F., Bekki, S., et al. (2022). Global perturbation of stratospheric water and aerosol burden by Hunga eruption. *Communications Earth & Environment*, *3*(1), 316. https://doi.org/10.1038/s43247-022-00652-x

Knox, J. A. (1998). On converting potential temperature to altitude in the middle atmosphere. *Eos Trans. AGU*, *79*(31), 376–378. https://doi.org/10.1029/98eo00290

Lambert, A., Livesey, N., & Read, W. (2020a). MLS/Aura level 2 nitrous oxide (N2O) mixing ratio V005 [dataset]. Goddard Earth Sciences Data and Information Services Center (GES DISC). https://doi.org/10.5067/Aura/MLS/DATA2515

Lambert, A., Livesey, N., Read, W., & Fuller, R. (2021a). MLS/Aura level 3 daily binned nitrous oxide (N_2O) mixing ratio on zonal and similar grids V005 [dataset]. Goddard Earth Sciences Data and Information Services Center (GES DISC). https://doi.org/10.5067/Aura/MLS/DATA3575

Lambert, A., Livesey, N., Read, W., & Fuller, R. (2021b). MLS/Aura level 3 daily binned water vapor (H_2O) mixing ratio on zonal and similar grids V005 [Dataset]. Goddard Earth Sciences Data and Information Services Center (GES DISC). https://doi.org/10.5067/Aura/MLS/DATA3568

Lambert, A., Read, W., & Livesey, N. (2020b). MLS/Aura Level 2 water vapor (H_2O) mixing ratio V005 [dataset]. Goddard Earth Sciences Data and Information Services Center (GES DISC). https://doi.org/10.5067/Aura/MLS/DATA2508

Lawrence, Z. D., Manney, G. L., & Wargan, K. (2018). Reanalysis intercomparisons of stratospheric polar processing diagnostics. *Atmospheric Chemistry and Physics*, *18*, 13547–13579. https://doi.org/10.5194/acp-18-13547-2018

Lee, J. N., Wu, D. L., Manney, G. L., Schwartz, M. J., Lambert, A., Livesey, N. J., et al. (2011). Aura Microwave Limb Sounder observations of the polar middle atmosphere: Dynamics and transport of CO and H_2O. *Journal of Geophysical Research*, *116*(D5), D05110. https://doi.org/10.1029/2010JD014608

Legras, B., Duchamp, C., Sellitto, P., Podglajen, A., Carboni, E., Siddans, R., et al. (2022). The evolution and dynamics of the Hunga Tonga–Hunga Ha'apai sulfate aerosol plume in the stratosphere. *Atmospheric Chemistry and Physics*, *22*(22), 14957–14970. https://doi.org/10.5194/acp-22-14957-2022

Livesey, N. J., Read, W. G., Wagner, P. A., Froidevaux, L., Lambert, A., Manney, G. L., et al. (2020). *EOS MLS version 5.0x level 2 and 3 data quality and description document (Tech. Rep.)*. JPL. Retrieved from http://mls.jpl.nasa.gov/

Manney, G. L., & Millán, L. F. (2007). Derived meteorological products for Aura Microwave Limb Sounder and other satellite datasets. Retrieved from https://mls.jpl.nasa.gov/eos-aura-mls/dmp

Manney, G. L., Santee, M. L., Livesey, N., Read, W., & Fuller, R. (2021). MLS/Aura level 3 daily binned nitric acid (HNO3) mixing ratio on zonal and similar grids V005 [Dataset]. Goddard Earth Sciences Data and Information Services Center (GES DISC). https://doi.org/10.5067/Aura/MLS/DATA3571

Manney, G. L., Zurek, R. W., O'Neill, A., & Swinbank, R. (1994). On the motion of air through the stratospheric polar vortex. *Journal of the Atmospheric Sciences*, *51*(20), 2973–2994. https://doi.org/10.1175/1520-0469(1994)051<2973:otmoat>2.0.co;2

Millán, L., Santee, M. L., Lambert, A., Livesey, N. J., Werner, F., Schwartz, M. J., et al. (2022). The Hunga Tonga-Hunga Ha'apai hydration of the stratosphere. *Geophysical Research Letters*, *49*(13), e2022GL099381. https://doi.org/10.1029/2022GL099381

Nakamura, N. (1996). Two-dimensional mixing, edge formation, and permeability diagnosed in area coordinates. *Journal of the Atmospheric Sciences*, *53*(11), 1524–1537. https://doi.org/10.1175/1520-0469(1996)053<1524:tdmefa>2.0.co;2

Randel, W. J., Moyer, E., Park, M., Jensen, E., Bernath, P., Walker, K., & Boone, C. (2012). Global variations of HDO and HDO/H2O ratios in the upper troposphere and lower stratosphere derived from ACE-FTS satellite measurements. *Journal of Geophysical Research*, *117*(D6), D06303. https://doi.org/10.1029/2011JD016632

Ray, E. A., Moore, F. L., Elkins, J. W., Hurst, D. F., Romashkin, P. A., Dutton, G. S., & Fahey, D. W. (2002). Descent and mixing in the 1999-2000 northern polar vortex inferred from in situ tracer measurments. *Journal of Geophysical Research*, *107*(D20), 8285. https://doi.org/10.1029/2001JD000961

Santee, M. L., Lambert, A., Manney, G. L., Livesey, N. J., Froidevaux, L., Neu, J. L., et al. (2022). Prolonged and pervasive perturbations in the composition of the Southern Hemisphere midlatitude lower stratosphere from the Australian New Year's fires. *Geophysical Research Letters*, *49*(4), e2021GL096270. https://doi.org/10.1029/2021GL096270

Santee, M. L., Livesey, N., Read, W., & Fuller, R. (2021). MLS/Aura level 3 daily binned chlorine monoxide (ClO) mixing ratio on zonal and similar grids V005 [dataset]. Goddard Earth Sciences Data and Information Services Center (GES DISC). https://doi.org/10.5067/Aura/MLS/DATA3535

Santee, M. L., MacKenzie, I. A., Manney, G. L., Chipperfield, M. P., Bernath, P. F., Walker, K. A., et al. (2008). A study of stratospheric chlorine partitioning based on new satellite measurements and modeling. *Journal of Geophysical Research*, *113*(D12), D12307. https://doi.org/10.1029/2007JD009057

Santee, M. L., Manney, G. L., Froidevaux, L., Livesey, N. J., Read, W. G., & Schwartz, M. J. (2011). Trace gas evolution in the lowermost stratosphere from Aura Microwave Limb Sounder measurements. *Journal of Geophysical Research*, *116*(D18), D18306. https://doi.org/10.1029/2011JD015590

Schoeberl, M. R., & Hartmann, D. L. (1991). The dynamics of the stratospheric polar vortex and its relation to springtime ozone depletions. *Science*, *251*(4989), 46–52. https://doi.org/10.1126/science.251.4989.46

Schoeberl, M. R., Lait, L. R., Newman, P. A., & Rosenfield, J. E. (1992). The structure of the polar vortex. *Journal of Geophysical Research*, *97*(D8), 7859–7882. https://doi.org/10.1029/91jd02168

Schoeberl, M. R., Wang, Y., Ueyama, R., Taha, G., Jensen, E., & Yu, W. (2022). Analysis and impact of the Hunga Tonga-Hunga Ha'apai stratospheric water vapor plume. *Geophysical Research Letters*, *49*(20), e2022GL100248. https://doi.org/10.1029/2022GL100248

Schoeberl, M. R., Wang, Y., Ueyama, R., Taha, G., & Yu, W. (2023). The cross equatorial transport of the Hunga Tonga-Hunga Ha'apai eruption plume. *Geophysical Research Letters*, *50*(4), e2022GL102443. https://doi.org/10.1029/2022GL102443

Schwartz, M., Froidevaux, L., Livesey, N., Read, W., & Fuller, R. (2021a). MLS/Aura level 3 daily binned ozone (O_3) mixing ratio on zonal and similar grids V005 [dataset]. Goddard Earth Sciences Data and Information Services Center (GES DISC). https://doi.org/10.5067/Aura/MLS/DATA/3105

Schwartz, M., Livesey, N., Read, W., & Fuller, R. (2021b). MLS/Aura level 3 daily binned temperature mixing ratio on zonal and similar grids V005 [dataset]. Goddard Earth Sciences Data and Information Services Center (GES DISC). https://doi.org/10.5067/Aura/MLS/DATA3580

Schwartz, M., Pumphrey, H., Livesey, N., & Read, W. (2020). MLS/Aura level 2 carbon monoxide (CO) mixing ratio V005 [Dataset]. Goddard Earth Sciences Data and Information Services Center (GES DISC). https://doi.org/10.5067/Aura/MLS/DATA2506

Sellitto, P., Podglajen, A., Belhadji, R., Boichu, M., Carboni, E., Cuesta, J., et al. (2022). November). The unexpected radiative impact of the Hunga Tonga eruption of 15th January 2022. *Communications Earth & Environment*, *3*(1), 1–10. https://doi.org/10.1038/s43247-022-00618-z

Sheese, P. E., & Walker, K. A. (2020). Data quality flags for ACE-FTS level 2 version 4.1/4.2 [Dataset]. Scholars Portal Dataverse. https://doi.org/10.5683/SP2/BC4ATC

Taha, G. (2020). OMPS-NPP L2 LP aerosol extinction vertical profile swath daily 3slit V2.1 [Dataset]. GES DISC. https://doi.org/10.5067/CX2B9NW6FI27

Taha, G., Loughman, R., Colarco, P. R., Zhu, T., Thomason, L. W., & Jaross, G. (2022). Tracking the 2022 Hunga Tonga-Hunga Ha'apai aerosol cloud in the upper and middle stratosphere using space-based observations. *Geophysical Research Letters*, *49*(19), e2022GL100091. https://doi.org/10.1029/2022GL100091

Vömel, H., Evan, S., & Tully, M. (2022). Water vapor injection into the stratosphere by Hunga Tonga-Hunga Ha'apai. *Science*, *377*(6613), 1444–1447. https://doi.org/10.1126/science.abq2299

Wargan, K., Weir, B., Manney, G. L., Cohn, S. E., & Livesey, N. J. (2020). The anomalous 2019 Antarctic ozone hole in the GEOS constituent data assimilation system with MLS observations. *Journal of Geophysical Research: Atmospheres*, *125*(18), e2020JD033335. https://doi.org/10.1029/2020JD033335

WMO. (2023). Scientific assessment of ozone depletion: 2022. *Global Ozone Res. and Monit. Proj. Rep.*, *55*.

Zawada, D. J., Rieger, L. A., Bourassa, A. E., & Degenstein, D. A. (2022). OMPS-NPP L2 LP USask aerosol extinction vertical profile swath daily V1.2 (1.2.0) [dataset]. Zenodo. https://doi.org/10.5281/zenodo.7293120

Zhu, Y., Bardeen, C. G., Tilmes, S., Mills, M. J., Wang, X., Harvey, V. L., et al. (2022). October). Perturbations in stratospheric aerosol evolution due to the water-rich plume of the 2022 hunga-Tonga eruption. *Communications Earth & Environment*, *3*(1), 248. https://doi.org/10.1038/s43247-022-00580-w

References From the Supporting Information

Boone, C., Bernath, P., Cok, D., Jones, S., & Steffen, J. (2020). Version 4 retrievals for the atmospheric chemistry experiment Fourier transform spectrometer (ACE-FTS) and imagers. *Journal of Quantitative Spectroscopy and Radiative Transfer*, *247*, 106939. https://doi.org/10.1016/j.jqsrt.2020.106939

Bourassa, A. E., Zawada, D. J., Rieger, L. A., Warnock, T. W., Toohey, M., & Degenstein, D. A. (2023). Tomographic retrievals of Hunga Tonga-Hunga Ha'apai volcanic aerosol. *Geophysical Research Letters*, *50*(3), e2022GL101978. https://doi.org/10.1029/2022GL101978

Haynes, P., & Shuckburgh, E. (2000). Effective diffusivity as a diagnostic of atmospheric transport 1. Stratosphere. *Journal of Geophysical Research*, *105*(D18), 22777–22794. https://doi.org/10.1029/2000jd900093

Manney, G. L., Harwood, R. S., MacKenzie, I. A., Minschwaner, K., Allen, D. R., Santee, M. L., et al. (2009). Satellite observations and modelling of transport in the upper troposphere through the lower mesosphere during the 2006 major stratospheric sudden warming. *Atmospheric Chemistry and Physics*, *9*(14), 4775–4795. https://doi.org/10.5194/acp-9-4775-2009

Manney, G. L., Millán, L. F., Santee, M. L., Wargan, K., Lambert, A., Neu, J. L., et al. (2022). Signatures of anomalous transport in the 2019/2020 Arctic stratospheric polar vortex. *Journal of Geophysical Research: Atmospheres*, *127*(20), e2022JD037407. https://doi.org/10.1029/2022JD037407

Sheese, P. E., Walker, K. A., Boone, C. D., Bourassa, A. E., Degenstein, D. A., Froidevaux, L., et al. (2022). Assessment of the quality of ACE-FTS stratospheric ozone data. *Atmospheric Measurement Techniques*, *15*(5), 1233–1249. https://doi.org/10.5194/amt-15-1233-2022

Taha, G., Loughman, R., Zhu, T., Thomason, L., Kar, J., Rieger, L., & Bourassa, A. (2021). OMPS LP version 2.0 multi-wavelength aerosol extinction coefficient retrieval algorithm. *Atmospheric Measurement Techniques*, *14*(2), 1015–1036. https://doi.org/10.5194/amt-14-1015-2021